



RESEARCH ARTICLE

10.1029/2021AV000519

Peer Review The peer review history for this article is available as a PDF in the Supporting Information.

Key Points:

- Expansion of urban areas causes losses of surface waters that extend in the neighboring region
- Surface water loss exponentially decreases as the distance from urban areas increases
- Climate controls the spatial distribution of surface water loss, with local versus widespread losses in temperate and continental versus arid areas

Supporting Information:

Supporting Information may be found in the online version of this article.

Correspondence to:

I. Palazzoli,
irene.palazzoli@unibo.it

Citation:

Palazzoli, I., Montanari, A., & Ceola, S. (2022). Influence of urban areas on surface water loss in the contiguous United States. *AGU Advances*, 3, e2021AV000519. <https://doi.org/10.1029/2021AV000519>

Received 1 JUL 2021

Accepted 25 OCT 2021



Author Contributions:

Conceptualization: I. Palazzoli, S. Ceola
Formal analysis: I. Palazzoli
Methodology: I. Palazzoli, S. Ceola
Software: I. Palazzoli
Writing – original draft: I. Palazzoli, A. Montanari, S. Ceola
Writing – review & editing: I. Palazzoli, A. Montanari, S. Ceola

© 2022. The Authors.

This is an open access article under the terms of the [Creative Commons Attribution-NonCommercial License](https://creativecommons.org/licenses/by-nc/4.0/), which permits use, distribution and reproduction in any medium, provided the original work is properly cited and is not used for commercial purposes.

Influence of Urban Areas on Surface Water Loss in the Contiguous United States

I. Palazzoli¹ , A. Montanari¹ , and S. Ceola¹ 

¹Department of Civil, Chemical, Environmental and Materials Engineering, Alma Mater Studiorum, Università di Bologna, Bologna, Italy

Abstract Urbanization is one of the main drivers of surface water loss, which implies a transition from water to land. However, it is still unclear how urban areas affect the spatial pattern of surface water loss. Here, we use remotely sensed data to analyze and model the decrease of surface water extent and, in particular, the frequency of surface water loss as a function of distance from urban areas across the contiguous United States (CONUS). We employ an exponential distance-decay model that confirms the presence of a higher frequency of surface water loss in the proximity of human settlements and provides innovative insights on surface water loss patterns at different spatial scales (i.e., river basins, water resource regions, and the CONUS). These spatial patterns are found to be influenced by climatic conditions, with more widely distributed losses in arid regions with respect to temperate and continental climates. Our results provide a new and deeper understanding of the spatial influence of urban areas on surface water loss, which could be effectively integrated in the definition of sustainable strategies for urbanization, water management, and surface water restoration, focused on both human and environmental water needs.

Plain Language Summary Urbanization is causing serious impacts on surface water resources, being among the main factors contributing to their conversion to land, here quantified in terms of surface water loss. Future scenarios of urban growth project increasing losses of surface water, with cascading negative effects for people and the environment. Here, we use satellite images to identify where surface water loss and human settlements are located across the contiguous United States and analyze and model their mutual interaction. We find that surface water loss is concentrated around cities and we define its spatial pattern in the neighboring region of urban areas with a mathematical model. We also observe that climate affects the distance-decay behavior, as in arid regions surface water loss is more spread with respect to temperate and continental climates. Our findings are essential to understand how urbanization affects the spatial distribution of surface water loss, therefore supporting the definition of planning strategies for water resource management that ensure water conservation and mitigate the impacts of urbanization on ecosystems.

1. Introduction

Surface water plays an essential role for freshwater supply and the preservation of freshwater ecosystems and functions (Dieter et al., 2018; Jenkins et al., 2010; Poff et al., 1997). Socioeconomic and technological development, water-management policies, and climate variability influence surface water resources (Averyt et al., 2013; Brown et al., 2019; Delpla et al., 2009; Duran-Encalada et al., 2017; Erler et al., 2019; Yigzaw & Hossain, 2016). In particular, human activities severely affect water bodies, as they compromise water quantity and quality, threaten ecological integrity, posing a serious challenge for sustainable development (Botter & Durighetto, 2020; Ferguson & Maxwell, 2012; Haddeland et al., 2006; Khatri & Tyagi, 2015; Liyanage & Yamada, 2017). Over the next decades surface water resources from rivers, lakes, reservoirs, and wetlands are projected to be gradually more impacted by increasing urban and economic growth and climate change (Boretti & Rosa, 2019; Lyons, 2014; McDonald et al., 2014; McGrane, 2016; Richter et al., 2013), with larger water demands for consumptive use, food production, and power generation (McDonald, Douglas et al., 2011; McDonald, Green et al., 2011; Okello et al., 2015; Yigzaw & Hossain, 2016).

Urban development affects the distribution of surface water through direct water abstraction from springs and rivers (Flörke et al., 2018), groundwater exploitation turning into increased infiltration (Wada et al., 2012), land drainage supporting agricultural development (Smedema et al., 2000), and increased evaporation induced by the urban heat island effect (Zhou et al., 2015). In turn, a reduction in the extent of surface water bodies close

to cities indicates an anthropogenic overstress on water resources which implies concerns on future water resources availability (McDonald et al., 2014). In the United States surface water accounts for more than 70% of total freshwater supply (Dieter et al., 2018), and with nearly 80% of population currently living in cities (Sun & Caldwell, 2015), urban areas place enormous pressure on surface water resources. Pekel et al. (2016) observed that even if surface water area across the US increased on average by 0.5% since 1984, growing water demands and drought conditions determined a 33% loss of the extent of surface water resources in the western region of the country (i.e., Arizona, California, Idaho, Nevada, Oregon, Utah). Future socio-economic and climate scenarios will likely exacerbate this situation (Baldocchi et al., 2019; Brown et al., 2019; Li, Sun, et al., 2020; Yigzaw & Hossain, 2016), as population increase is expected to cause a significant gap between water demand and supply in the future (Daher et al., 2019), and increasing temperatures will likely impact the hydrological cycle and water balance (Brown et al., 2019).

Even though the impacts of urbanization on the environment have been long studied, the consequences of urban development on water resources, and in particular the spatial interaction between urban areas and surface water loss distribution, are less known (Bigelow et al., 2017). In order to identify hotspots of localized and concentrated pressure on surface waters, which may produce negative effects on human life and the environment, it is necessary to unravel the spatial influence of human settlements on surface water loss (Boretti & Rosa, 2019; Padowski & Jawitz, 2012; Wada et al., 2016).

Earth Observation (EO) data have been widely employed to detect the extent of surface water and built-up areas, as well as to track their spatiotemporal variation (Corbane et al., 2019; Huang et al., 2018; Liu, Huang, et al., 2020; Marconcini et al., 2020; Pekel et al., 2016; Xiong et al., 2018). Geographical patterns identified in EO images reveal the spatial interaction between places. This interaction primarily depends on the geographical separation between two locations, since its intensity decreases with increasing distance. In spatial pattern analysis this behavior is known as the distance-decay effect, a fundamental concept extensively applied in human and urban geography (Fotheringham, 1981; Li, Gao, et al., 2020; Taylor, 1971; Yin et al., 2019).

Several studies on the proximity of human settlements to water have been carried out (Ceola et al., 2014; Fang & Jawitz, 2019; Fang et al., 2018; Liu, Yang, et al., 2021; Mård et al., 2018). However, the spatial interaction between cities and surface water loss and its modeling through the distance-decay concept still remain to be explored. Moreover, this aspect has not been investigated with EO data, despite the availability of many consistent global products that accurately describe surface water dynamics and urban growth.

Here, we present an innovative application of the distance-decay concept to evaluate the influence of urban areas on the spatial distribution of surface water loss across the contiguous United States (CONUS) by using data acquired from EO sensors. In our analysis, surface water loss is defined as a reduction in water frequency observations, regardless of the cause (i.e., anthropogenic or climatic) and loss magnitude, that generates the conversion from water to land. We considered two crucial questions, as illustrated in Figure 1: (a) where and how does urbanization cause surface water loss? And (b) how does surface water loss decline as the distance from human settlements increases? To address these questions, we extracted maps of surface water loss locations and built-up areas from EO data, and we examined the frequency of occurrence of surface water loss with respect to distance from urban areas in bins of 3 km across the CONUS. We finally analyzed the role of climate in the spatial interaction between urban areas and surface water loss to possibly identify distinct signatures in the frequency of occurrence of surface water loss.

An accurate understanding of the dynamics of the spatial interaction between urban areas and surface water loss distribution is fundamental to define ecologically sustainable solutions that ensure water conservation and ecosystem protection, with an emphasis on those strategies that allow to meet urban water demand and at the same time to prevent the depletion of surface water resources.

2. Study Area and Data

2.1. River Basins and Water Resource Regions Across the CONUS

The contiguous United States (CONUS) was selected as our study area. Following the delineation provided by the USGS (Seaber et al., 1987), this area includes 204 river basins (i.e., 4-digit hydrologic units, HUC-4s, also known as subregions) that form 18 water resource regions (WRRs), as shown in Figure 2. This area encompasses

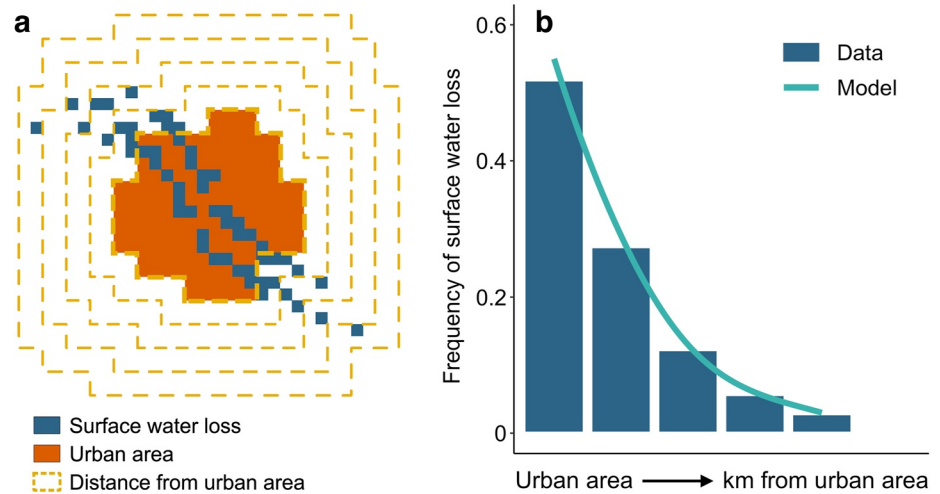


Figure 1. Schematic representation of the spatial interaction between surface water loss locations and urban areas hypothesized in this analysis. (a) Geographical distribution of surface water loss and urban areas across distance classes. (b) Comparison between observed and modeled frequency of occurrence of surface water loss, showing a decreasing pattern as the distance from urban areas increases.

an extensive and heterogeneous territory, characterized by broad topographic variations, wide-ranging surface water area extents, diverse urbanization levels, and different hydroclimatic conditions (Figure S1 in Supporting Information S1), here described by the main climatic zones of the Köppen climate classification system (Beck et al., 2018).

2.2. Surface Water Loss Map and Urbanization Map

To investigate the spatial influence of urban areas on surface water loss we processed datasets derived from EO data and defined two binary maps: the Surface Water Loss map and the Urbanization map (Palazzoli et al., 2021). The Surface Water Loss map identifies the geographical location of pixels that experienced a reduction in water frequency observations, leading to a conversion from water to land at the end of the period 1984–2018 (blue pixels in Figure 2). We obtained the Surface Water Loss map from the Surface Water Transitions layer of the Global Surface Water dataset (Pekel et al., 2016). This dataset classifies any surface water body open to the sky and larger than 30 m by 30 m as open water, including fresh and saltwater (Pekel et al., 2016), and it provides an unprecedented evaluation of surface water dynamics (Yamazaki & Trigg, 2016). We used the Surface Water Transitions layer because it describes the evolution of surface water state that took place between the first and last year of the observation period (1984 and 2018), showing any conversion among permanent surface water, seasonal surface water, and land (i.e., areas without any water). The class of transition assigned to each water pixel is defined based on the variation of its frequency of observation. We selected lost permanent, lost seasonal, ephemeral permanent, and ephemeral seasonal surface water pixels as representatives of locations that experienced surface water loss (i.e., water-land transition) during the time window 1984–2018 and we used them to define the Surface Water Loss map. Lost permanent (or seasonal) surface water indicates a conversion of permanent (or seasonal) water into land. Ephemeral permanent (or seasonal) surface water identifies locations where surface water resources are permanent (or seasonal) for some of the intervening years, but no water is detected in the first and last year of the observational period (Pekel et al., 2016). The whole study area includes more than 85 million pixels of surface water loss, of which lost permanent, lost seasonal, ephemeral permanent, and ephemeral seasonal surface water constitute 13%, 29%, 2%, 56%, respectively. We analyzed the frequency with which surface water was observed between 1984 and 2018 in the selected classes of water transition (Figure S2 in Supporting Information S1), as derived from the Water Occurrence layer of the Global Surface Water dataset (Pekel et al., 2016). As expected, water occurrence values decrease from lost permanent, to ephemeral permanent, lost seasonal, and ephemeral seasonal (Figures S3 and S4 in Supporting Information S1), with median values equal to 50%, 30%, 18%, and 10%, respectively. This outcome shows a significant presence of water in correspondence of the surface water loss pixels during the observation period, which resulted to be lost in 2018.

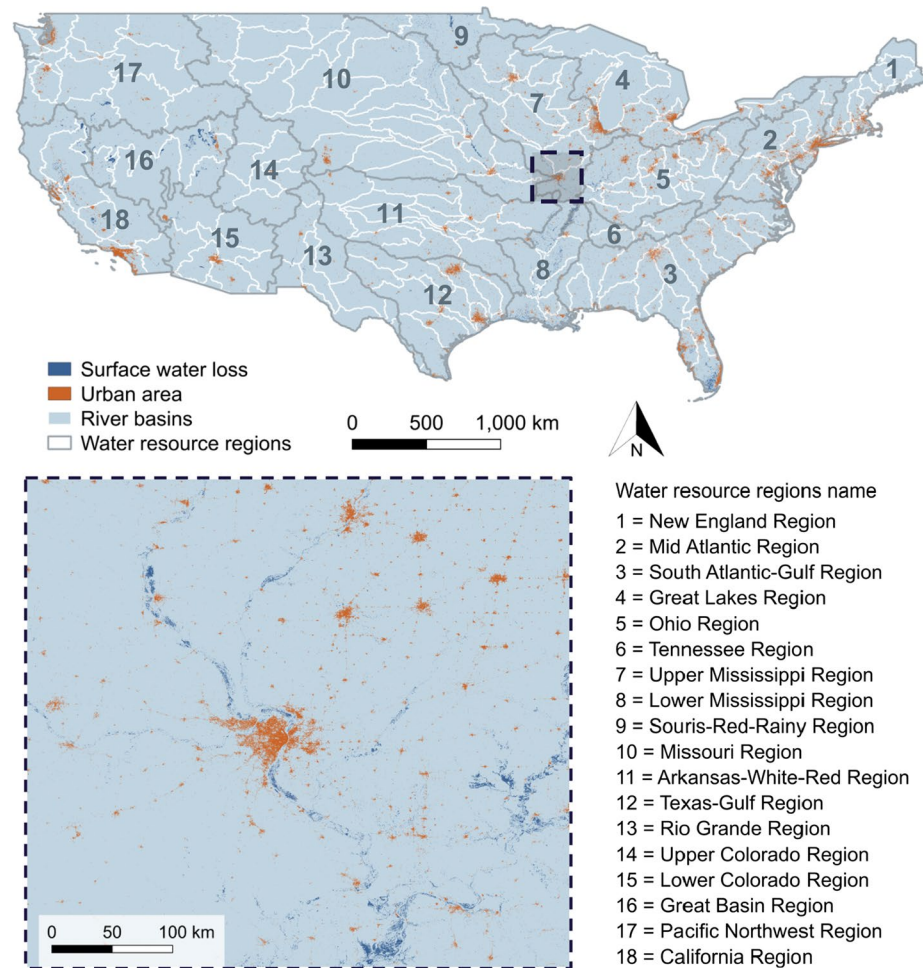


Figure 2. Surface water loss locations and urban areas across river basins and water resource regions of the CONUS. Locations that experienced surface water loss are colored in blue. The extent of urban areas is shown in orange. The boundaries of the 204 HUC-4s river basins are depicted in white, while the 18 water resource regions are numbered and highlighted with a bold gray line. The dark blue dashed box represents a zoom in over the area around the city of Saint Louis and the Mississippi River.

The Urbanization map describes the most recent extent of urban areas (up to 2014, orange pixels in Figure 2). We generated the Urbanization map from the GHS-BUILT layer of the Global Human Settlement dataset (Corbane et al., 2019). The GHS-BUILT layer provides a multitemporal classification of built-up land over time with a resolution of 30 m, showing the location of built-up areas developed during four epochs (until 1975, from 1975 to 1990, from 1990 to 2000, and from 2000 to 2014), no built-up land, and water surface. Pixels classified as built-up in each epoch define the Urbanization map.

3. Methods

3.1. Surface Water Loss From Urban Areas: Observed Frequency of Occurrence

We estimated the geographical distance of surface water loss pixels from urban areas using the Euclidean distance, that is, the length of a straight line connecting pairs of locations. As a conservative approach, we assumed that urban areas can access all nearby surface water resources leading to a conversion from water to land, that is, surface water loss. Although other physical factors (such as terrain elevation, road networks, and water supply systems) might have been considered in the definition of the distance metric, we adopted the Euclidean distance since it provides an objective and global reference while also being a relevant design driver for technological networks. Moreover, it is the most common measure of geographical distance used in distance-decay applications

(Artell et al., 2019; Goldmann et al., 2016; Halás et al., 2014). Finally, the Euclidean distance allows to define a simple model that reproduces the observed spatial interaction between surface water loss and urbanization, avoiding too many independent variables that would otherwise enter the distance-decay function, increasing its level of complexity and related model uncertainty.

We measured the Euclidean distance of surface water loss from the boundaries of urban areas (Figure 1a) across each spatial aggregation x here considered (i.e., river basin, $x = b$, water resource region, $x = WRR$, and the CONUS, $x = CONUS$). Afterward, we divided the Euclidean distance values in bins having a constant width and we aggregated counts of surface water loss pixels within each distance bin d_{ij} to calculate the frequency of occurrence of surface water loss $f_x(d_{ij})$ (histogram in Figure 1b) as follows:

$$f_x(d_{ij}) = \frac{swl_x(d_{ij})}{swl_{x,tot}} \quad (1)$$

where $swl_x(d_{ij})$ is the count of surface water loss locations in the considered spatial aggregation x between distances i and j (with i and j ranging from 0 to $d_{x,max}$, i.e., the maximum distance reached in x), while $swl_{x,tot}$ is the total count of surface water loss locations observed inside the considered spatial aggregation x .

We selected a 3 km wide distance bin based on the results of a sensitivity analysis that compared the frequency of occurrence of surface water loss obtained with aggregations at 1, 3, and 5 km wide distance bins. The width of 3 km resulted to be the optimal compromise between noise reduction and level of detail (Figure S5 in Supporting Information S1). This aggregation was applied until 99 km of distance from urban areas (i.e., 0–3, 3–6, ..., 96–99 km distance bin).

We also computed the observed average distance of surface water loss locations from urban areas, $\langle d_x \rangle$, across each spatial aggregation x as follows:

$$\langle d_x \rangle = \frac{\sum_{k=1}^{swl_x} d_k}{swl_{x,tot}} \quad (2)$$

where d_k is the distance associated to a generic surface water loss location.

3.2. Surface Water Loss From Urban Areas: Distance-Decay Model

By assuming that the influence of urbanization on surface water loss locations declines as the distance of these locations from urban areas increases, we defined a probabilistic model capable of reproducing this distance-decay behavior (solid line in Figure 1b). We modeled the distance-decay with a truncated exponential probability distribution, which describes a decreasing trend of the frequency of occurrence of surface water loss pixels, so that the maximum probability of finding surface water loss occurs at a distance close to the urban region and exponentially declines with increasing distance. We selected the truncated exponential probability distribution because the exponential decay is among the most employed distance-decay functions, with several applications in different fields (Chen & Huang, 2018; Figueiredo et al., 2015; Martínez & Viegas, 2013; Zhang, 2011). We adopted the truncated version because, by definition, the distance reaches a finite maximum value $d_{x,max}$ in each spatial aggregation x .

The probability of occurrence of surface water loss locations as a function of the distance from urban areas, $p_x(d_{ij})$, across each spatial aggregation x reads as follows:

$$p_x(d_{ij}) = \alpha_x e^{-\beta_x d_{ij}} \quad (3)$$

where α_x [-] is the frequency of occurrence of surface water loss locations in the initial 3 km wide distance bin (0–3 km), and β_x (>0 [km^{-1}]) represents the decay rate of the model, describing the rate of decline in spatial interaction. The higher β_x , the steeper is the decrease in $p_x(d_{ij})$ with increasing distance from urban areas.

We estimated α_x and β_x in Equation 3 through a non-linear regression of the probability of occurrence $p_x(d_{ij})$ versus the observed frequency of surface water loss locations $f_x(d_{ij})$, by assuming that at least values in three distance bins are available in order to get a robust fit ($d_{x,max} > 6$ km). The goodness of fit was assessed through the evaluation of the Pearson's correlation coefficient r . In addition, we calculated the standard error associated to the

model fit derived for each spatial aggregation x , to evaluate the distance of observed values from the regression line of the model. This value was used to estimate the prediction interval with 5% significance level, therefore providing an estimate for prediction uncertainty.

Furthermore, we compared the decay of surface water loss to the decay of the overall extent of surface water with distance from urban areas at the river basin level to further test if more surface water loss is occurring close to urban areas, rather than far from them. We extracted the overall extent of surface water from the Water Extent layer of the Global Surface Water dataset (Pekel et al., 2016). To avoid biases due to large water bodies, we calculated the Euclidean distance from urban areas only at the boundaries of surface water bodies (these resources are also the most likely to be exhausted because of human withdrawals). Similarly to what we did for the surface water loss decay, we performed a non-linear regression and we evaluated the distance-decay model parameters, based on the overall extent of surface water. A decay rate of surface water loss β_b larger (smaller) than the decay rate of the overall extent of surface water β_b^{sw} indicates an area where more surface water loss is occurring close to (far from) urban areas.

Finally, we analytically derived from Equation 3 the theoretical average distance of surface water loss locations from urban areas (i.e., the expected value of the truncated exponential distribution), $\langle \hat{d}_x \rangle$, across each spatial aggregation x as follows:

$$\langle \hat{d}_x \rangle = \frac{1 - e^{-\beta_x d_{x,max}} (1 + \beta_x d_{x,max})}{\beta_x (1 - e^{-\beta_x d_{x,max}})} \quad (4)$$

To check for the reliability of Equation 3 in reproducing the observed distance-decay pattern of surface water loss locations, we compared the observed and the theoretical average distances, $\langle d_x \rangle$ from Equation 2 and $\langle \hat{d}_x \rangle$ from Equation 4, for each spatial aggregation x .

4. Results

4.1. Observed Spatial Interaction Between Surface Water Loss and Urban Areas

We consistently found that the observed frequency of occurrence of surface water loss locations decreases as the distance from urban areas increases across the whole study area, at river basin, water resource region, and CONUS levels. This result applies to any geographical position, climatic zone, and physiographic properties. Figure 3 clearly shows this outcome for the CONUS (diamonds in Figure 3b) and for four water resource regions and related river basins (circles in Figures 3c–3j). Similar results were also found for the remaining river basins and water resource regions, thus confirming that surface water losses are consistently located in the proximity of urban areas (see Figure S6 in Supporting Information S1 for the remaining 14 water resource regions).

4.2. Spatial Interaction Between Surface Water Loss and Urban Areas: Distance-Decay Model Application

We then computed the probability of occurrence of surface water loss locations as a function of the distance from urban areas. The application of Equation 3, based on the selected 3 km wide distance bin, shows that all 18 water resource regions and 191 river basins (96% of the total) are successfully fitted by the distance-decay model (Figures 3a and S6 in Supporting Information S1), with r values ranging from 0.974 to 0.999 and from 0.676 to 0.999, for the water resource regions and the river basins, respectively. In the remaining 13 river basins, Equation 3 could not be applied at the selected 3 km wide distance bin because of data paucity (i.e., $d_{x,max} \leq 6$ km, meaning that data are available in less than three distance bins). However, for these river basins, Figure 3a shows r values ($r \geq 0.952$) obtained with 1 km wide distance bins (see river basins with a dark gray line pattern). Data and model comparison for the four aforementioned water resource regions and related river basins are shown in Figures 3b–3j. A statistically significant fit ($r = 0.997$) is also found when the distance-decay model is applied to the CONUS, proving the reliability of our mathematical interpretation of the influence of urbanization on the spatial distribution of surface water loss at different levels of spatial aggregation. Moreover, by comparing the decay rate of surface water loss (β_b) to the one associated to the overall extent of surface water (β_b^{sw}), we found that in the aforementioned 191 river basins the decay of surface water loss is steeper than the decay of the overall

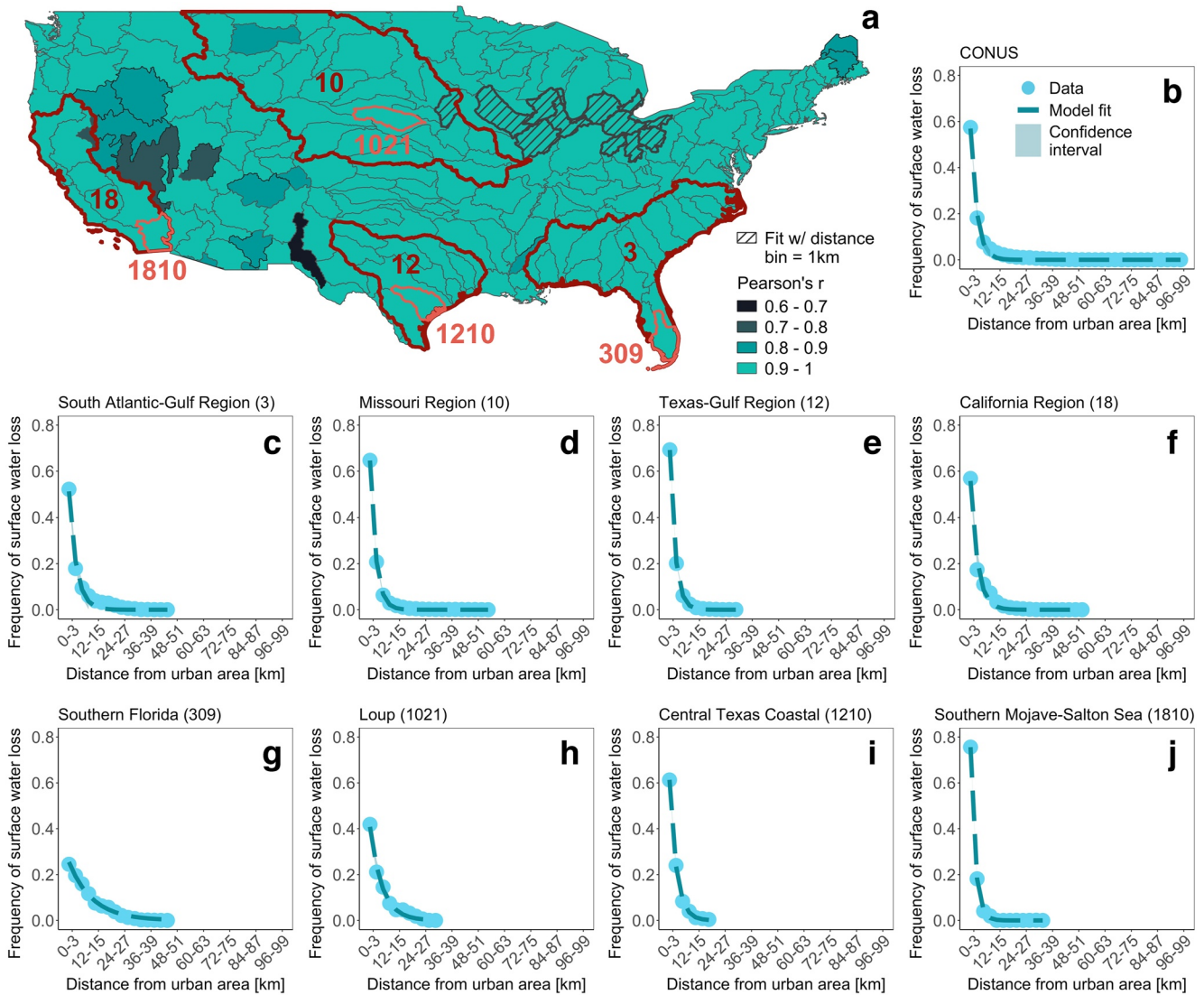


Figure 3. Performance of the distance-decay model reproducing the observed frequency of occurrence of surface water loss from urban areas, based on a 3 km wide distance bin. (a) Spatial distribution of model performance, where river basins are colored according to their Pearson's correlation coefficient. River basins where the model fit is obtained with a distance bin of 1 km are indicated with a dark gray line pattern. Water resource regions (3, 10, 12, 18) and river basins (309, 1021, 1210, 1810) shown in panels c–j are highlighted with a thicker border. (b) Frequency of occurrence of surface water loss locations and model fit obtained for the CONUS. Confidence intervals represent the standard error associated to the model fit. (c–f) Frequency of occurrence of surface water loss locations and model fit obtained for the selected water resource regions. (g–j) Frequency of occurrence of surface water loss locations and model fit obtained for the selected river basins.

extent of surface water (Figures S7 and S8 in Supporting Information S1). This result clearly demonstrates that more surface water loss is occurring close to urban areas consistently in all the rivers basins of the CONUS.

Table 1 provides the main physical and climatic properties and model parameters for the CONUS and the selected water resource regions and river basins shown in Figure 3. The entire list of the main physical and climatic properties and model parameters for the 18 water resource regions and the 204 river basins can be found in Table S1.

We tested the reliability of our distance-decay model by comparing the observed and theoretical average distances of surface water loss locations from urban areas ($\langle d_y \rangle$ and $\langle \hat{d}_x \rangle$ from Equations 2 and 4) in each level of spatial aggregation here considered, namely river basins, water resource regions, and CONUS. In what follows, results refer only to the CONUS, the 18 water resource regions, and the 191 river basins whose data were fitted by Equation 3 using a 3 km wide distance bin. Figure 4a shows that pairs of observed and theoretical average distances at the river basin level are well correlated, where the slope of the linear regression is equal to 1.00 ($R^2 = 0.84$,

Table 1

Main Physical and Climatic Properties and Model Fit Results, Based on a 3 km Wide Distance Bin, for the CONUS and Four Representative Water Resource Regions and Related River Basins

Water resource region/river basin name (ID)	Area [km ²]	Average elevation ± std dev [m]	Climatic regions and coverage percentage	α_x	β_x	r	$\langle d_x \rangle$	$\langle \hat{d}_x \rangle$
				[-]	[km ⁻¹]		[km]	[km]
CONUS	7,744,303	-	Continental (40.47%), Arid (33.67%), Temperate (25.41%), Tropical (0.27%), Polar (0.18%)	0.570	0.348	0.997	5.304	2.870
South Atlantic-Gulf Region (3)	695,951	110 ± 118	Tropical (59.48%), Temperate (40.52%)	0.512	0.295	0.994	5.407	3.391
Southern Florida (309)	42,136	12 ± 9	Tropical (59.48%), Temperate (40.52%)	0.255	0.093	0.996	8.992	10.140
Missouri Region (10)	1,323,835	996 ± 620	Continental (99.94%), Temperate (0.06%)	0.646	0.376	1.000	3.653	2.658
Loup (1021)	39,214	825 ± 188	Continental (95.29%), Arid (4.71%)	0.408	0.182	0.995	5.946	5.380
Texas-Gulf Region (12)	464,006	370 ± 348	Arid (85.42%), Temperate (14.58%)	0.692	0.407	1.000	2.703	2.457
Central Texas Coastal (1210)	44,227	160 ± 170	Temperate (99.94%), Arid (0.06%)	0.613	0.318	1.000	3.189	3.099
California Region (18)	416,156	888 ± 724	Temperate (77.67%), Arid (21.74%), Continental (0.59%)	0.558	0.312	0.993	4.245	3.202
Southern Mojave-Salton Sea (1810)	41,361	548 ± 470	Arid (93.38%), Temperate (6.4%), Continental (0.22%)	0.756	0.475	1.000	2.244	2.103

Note. α_x and β_x are the distance-decay model parameters; r is the Pearson's correlation coefficient; $\langle d_x \rangle$ and $\langle \hat{d}_x \rangle$ are the observed and theoretical average distance, respectively. The first row reporting the values for the CONUS does not contain any ID nor the elevation with its standard deviation, which is not a significant information for such a large area.

p -value \ll 0.05). A comparable and statistically significant correlation is also found for the 18 water resource regions (slope = 1.06, $R^2 = 0.87$, p -value \ll 0.05). The black diamond depicting the average distances for the CONUS falls marginally under the regression lines for river basins and water resource regions, meaning that our distance-decay model underestimates the observed distance at which on average surface water loss occurs at the continental scale (Table 1). Results from the linear correlation demonstrate the consistency of our model in reproducing the observed spatial pattern, as the truncated exponential probability distribution is able to predict

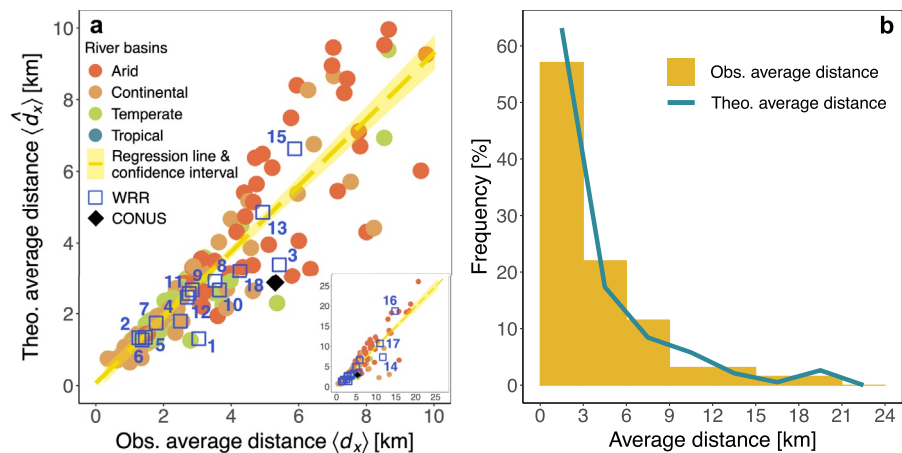


Figure 4. Comparison between the observed and theoretical average distance of surface water loss locations from urban areas ($\langle d_x \rangle$ and $\langle \hat{d}_x \rangle$) based on a 3 km wide distance bin and their frequency distribution. (a) Correlation between observed and theoretical average distances of surface water loss locations. Results from the three levels of spatial aggregation (river basins, water resource regions, and CONUS) are shown. Circles (whose color identifies the prevalent climatic region) show pairs of observed and theoretical distances obtained for the 191 river basins, blue squares are used to represent the 18 water resource regions (WRRs), while the black diamond identifies the same distances calculated for the CONUS. The linear regression between observed and theoretical distances at the river basin level is depicted by the yellow dashed line ($\langle \hat{d}_b \rangle = -0.13 + 1.00 \langle d_b \rangle$) and its coefficient of determination R^2 is 0.84. The light yellow area represents the 95% confidence interval of the linear regression. The linear regression between observed and theoretical distances at the water resource region level (not shown) is the following: $\langle \hat{d}_{WRR} \rangle = -0.73 + 1.06 \langle d_{WRR} \rangle$. (b) Frequency distribution of observed and theoretical average distances of surface water loss locations at the river basin level.

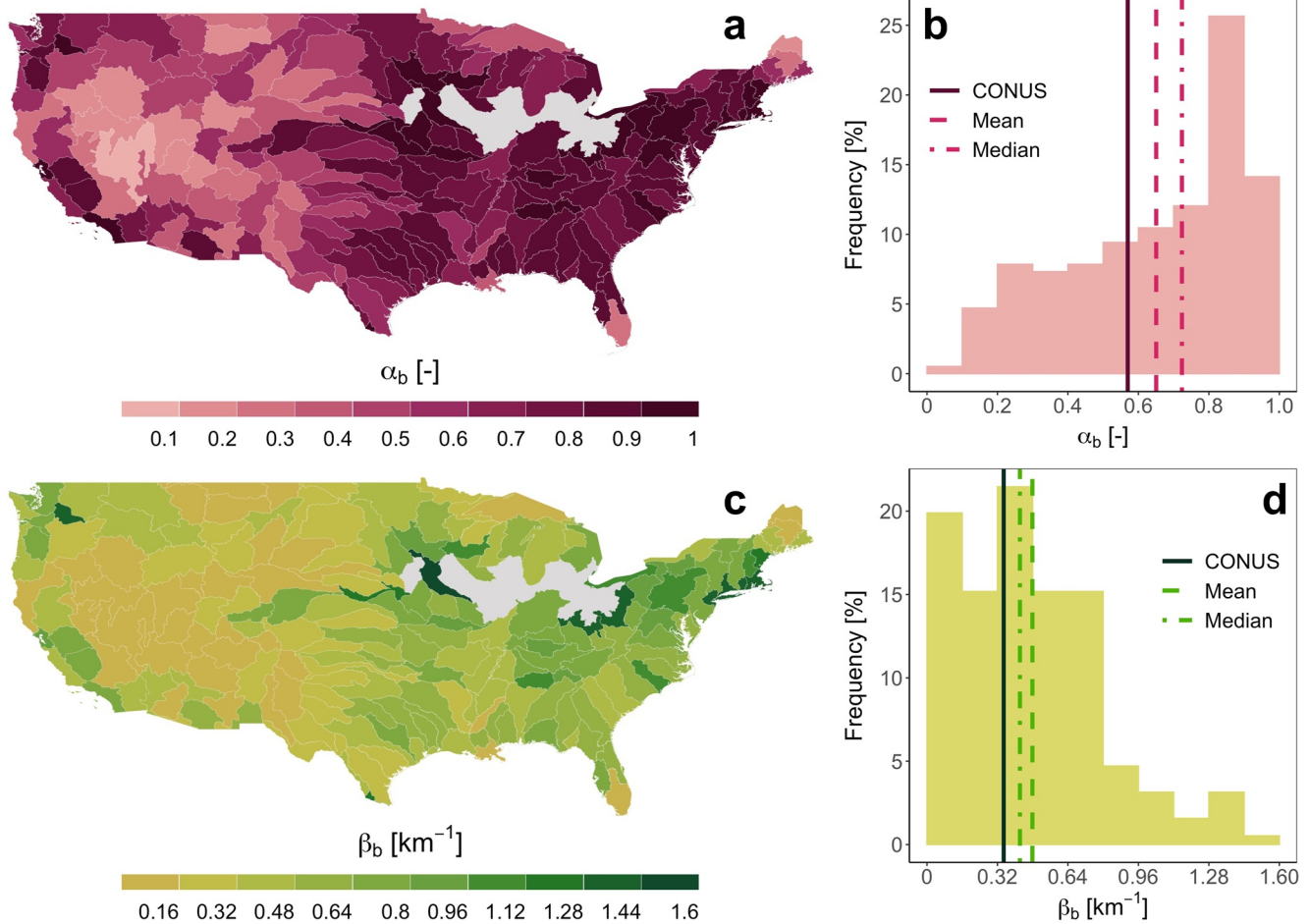


Figure 5. Spatial variability and frequency distribution of α_b and β_b parameters of the distance-decay model based on a 3 km wide distance bin and applied at the river basin level. (a) Spatial variability of α_b . River basins that are not fitted by the model using a 3 km wide distance bin are indicated in light gray. (b) Frequency distribution of α_b . The dashed line and the dot-dash line represent the mean and the median values, respectively, as derived from river basins, while the solid line depicts α_{CONUS} . (c) The same as panel a, but for the decay rate β_b . (d) The same as panel b, but for the decay rate β_b .

the distance from urban areas at which on average surface water loss may occur. We noticed that more than half of the river basins (109 out of 191) has an observed average distance smaller than 3 km (first bin of the histogram in Figure 4b).

To gain a deeper insight into the distance-decay behavior detected in our study area, we further analyzed the spatial variability and the frequency distribution of the model parameters α_x and β_x . Higher values of α_x and β_x imply a more concentrated loss of surface waters in the proximity of urban areas and a quicker decrease in surface water loss frequency as the distance from urban areas increases, respectively. As before, results refer only to the 18 water resource regions and 191 river basins for which Equation 3 fitted the data using a 3 km wide distance bin (i.e., river basins with a line pattern in Figure 3a are excluded). Values of α_b , as derived from river basins, range from 0.095 to 0.990, with the highest values found in river basins located in the eastern part of the CONUS and partly along the West Coast (Figure 5a), where the largest surface water withdrawals occurred (Dieter et al., 2018). Mean and median values of α_b are 0.651 and 0.724, respectively (Figure 5b), meaning that 72% of the river basins presents more than half of surface water loss within 3 km from urban areas. In the 18 water resource regions α_{WRR} ranges from 0.151 to 0.908, with a mean value of 0.610 and a median equal to 0.666 (Figure S12a in Supporting Information S1). For the CONUS, α_{CONUS} equals 0.570, confirming the concentration of surface water loss in the immediate proximity of urban areas. Regarding the decay rate β_x , values at the river basin level β_b range from 0.028 to 1.546 km^{-1} , with the highest values mainly found across the eastern part of the CONUS (Figure 5c), where most of urban areas are located (US Census, 2021). Mean and median values are 0.479 km^{-1}

and 0.422 km^{-1} , respectively, with the majority of river basins (92%) showing a value smaller than 1 km^{-1} (Figure 5d). In the remaining 8% of the river basins, where $\beta_b > 1 \text{ km}^{-1}$, a rapid decrease of surface water loss in space is found, indicating that the interaction between human settlements and surface water resources takes place over a shorter distance and thus only surface water resources close to cities are affected by urban areas. In the 18 water resource regions β_{WRR} ranges from 0.050 to 0.790, with a mean value of 0.407 and a median equal to 0.376 (Figure S12b in Supporting Information S1). For the CONUS, β_{CONUS} is equal to 0.348 km^{-1} . Results based on 1 and 5 km wide distance bins are shown in Figures S9 and S10 in Supporting Information S1 for river basins, and in Figures S11 and S13 in Supporting Information S1 for water resource regions.

We also tested if the variability of α_b and β_b model parameters reflects heterogeneities of urban attributes, such as total urban population, urban population change, and urban area change. To this aim, we extracted data of urban population and urban area from the GHS-POP and GHS-BUILT layers provided by the Global Human Settlement dataset (Corbane et al., 2019). Since population and built-up area data from GHS are available only for 1975, 1990, 2000, and 2015 (2014 for built-up area), we assumed that urban population detected in 1990 and 2015 and urban area found in 1990 and 2014 are a reasonable representation of the urban population and the level of urbanization during the first and last year of the period 1984–2018. The difference between urban population (or urban area) values in 2015 (or 2014) and 1990 was used to quantify urban population (or urban area) change. The general spatial distribution of urban population in 2015, urban population change, and urban area change at the river basin scale (Figure S14 in Supporting Information S1) is in agreement with the spatial trend observed for our model parameters α_b and β_b at the river basin level (Figures 5a and 5c), with higher urban population in 2015, urban population change, and urban area change along the East and West Coast. Indeed, when we represent the urban population in 2015, the urban population change and urban area change values against α_b and β_b parameters (Figure S15 in Supporting Information S1), we find a mild correlation between these variables, with the highest coefficient of determination R^2 found for the total urban population of 2015 and urban area change. Finally, we calculated the maximum extent of urban agglomerations in each river basin of the CONUS to inspect whether river basins having larger urban clusters experienced a more pronounced loss in surface water close to their urban areas. An evident influence of the maximum extent of urban clusters did not emerge from our analysis (Figures S16 and S17 in Supporting Information S1). However, we found that as the variability (i.e., the interquartile range) and the 75th percentile of the extent of urban agglomerations increase, the decay rate β_b increases as well (Figure S18 in Supporting Information S1), highlighting the presence of a steeper decay in surface water loss moving away from urban areas in river basins having larger urban agglomerations.

4.3. Influence of Climate

To investigate the role played by climate, we examined the spatial distribution of surface water loss locations and the associated variability of the model parameters α_b and β_b over the main Köppen climatic zones, that is, tropical, arid, temperate, continental, and polar (Beck et al., 2018). We found that more than one third of the surface water loss locations (37.13%) are located in the temperate region, with the remaining falling in the arid (29.37%), continental (27.5%), and tropical (5.99%) regions. Less than 0.01% of surface water loss occurs within the polar zone, which was not considered for further analysis. We then analyzed the variability of model parameters α_b and β_b in the climatic zones where locations of surface water loss are found, and calculated their weighted average associated to each climatic region (Figure 6). For a given climatic zone and river basin, the weight is defined as the ratio between the number of surface water loss locations within the portion of basin in that climatic zone (i.e., locations sharing the same values of α_b and β_b) and the total number of surface water loss locations found in the same climatic region.

The highest values of α_b and β_b parameters are found in the temperate and continental climatic regions. In the continental region, the weighted average of α_b is equal to 0.736 (1st, 2nd, 3rd quartiles equal to 0.692, 0.728, and 0.891, respectively), while the weighted average of β_b is equal to 0.527 (1st, 2nd, 3rd quartiles equal to 0.393, 0.410, and 0.732, respectively). The temperate region shows slightly smaller values, with the weighted average of α_b equal to 0.699 (1st, 2nd, 3rd quartiles equal to 0.633, 0.730, and 0.810, respectively), and the weighted average of β_b equal to 0.439 (1st, 2nd, 3rd quartiles equal to 0.362, 0.409, and 0.545, respectively). Across these two climatic zones, characterized by abundant water resources, we found that surface water loss is concentrated close to urban areas (i.e., the majority of surface water loss is located within a 3 km distance) and its frequency of occurrence is rapidly decreasing in space. Therefore, localized and concentrated impacts of urban areas on surface water loss

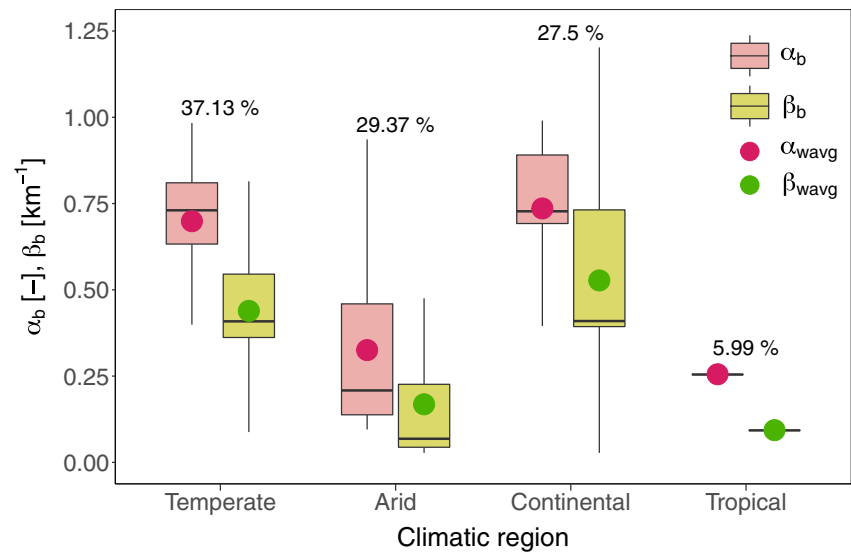


Figure 6. Variability of α_b and β_b parameters of the distance-decay model applied at the river basin level across the Köppen climatic regions (Beck et al., 2018) in the CONUS. The boxplot edges indicate the first and third quartiles, with the thick horizontal line representing the median value. Colored circles illustrate the weighted average of the parameters associated to each climatic region. The percentage of surface water loss locations falling in each climatic region is also indicated.

are typical of temperate and continental climatic regions, as also shown in Figure 4a where pairs of theoretical and observed average distance of surface water loss are colored based on the prevailing climatic region found in each river basin.

The arid region presents significantly smaller values of α_b and β_b parameters. In particular, the weighted average of α_b is equal to 0.325 (1st, 2nd, 3rd quartiles equal to 0.138, 0.208, and 0.459, respectively), while the weighted average of β_b is equal to 0.168 (1st, 2nd, 3rd quartiles equal to 0.044, 0.068, and 0.226, respectively). Across the arid region, characterized by a limited availability of surface water resources, we found that surface water loss is more uniformly distributed across all distance classes, with only a 16% of surface water loss within a 3 km distance from urban areas on average. Indeed, the frequency of occurrence of surface water loss in space shows a decreasing trend, although dampened when compared to temperate and continental regions. Arid climates are therefore characterized by more distributed impacts of urban areas on surface water loss, which typically affect larger areas around cities (see also Figure 4a).

The tropical region shows the lowest average values of α_b (0.255) and β_b (0.093 km⁻¹). However, surface water loss locations associated to this climatic region belong to one river basin only, thus limiting its representativeness.

Finally, we compared the decay rate of surface water loss (β_b) to the one associated to the overall extent of surface water (β_b^{sw}) and assessed their distribution across the Köppen climatic regions. We found that β_b^{sw} values are consistently smaller than β_b values across each climatic zone (Figure S19 in Supporting Information S1).

5. Discussion and Conclusions

Human pressure on surface water is increasing globally and especially on river systems (Ceola et al., 2019; Wada et al., 2013). By 2050 about 70% of the global population is expected to reside in cities (United Nations, 2019). Under this scenario the resulting process of urban sprawl will likely affect both the quantity and quality of water resources surrounding urban areas worldwide (Boretti & Rosa, 2019; McDonald et al., 2014; Padowski & Jawitz, 2012).

A substantial reduction in water frequency observations close to urban areas, indicative of surface water loss, can produce environmental, social, and economic impacts whose effects are going to influence increasingly larger areas (McDonald et al., 2014; Padowski & Gorelick, 2014; Richter et al., 2013). As urban population grows and urban area expands, local surface water could be lost due to several human-induced processes, such

as increasing water abstraction, groundwater exploitation, land drainage, and increased evaporation, with serious consequences for the integrity of freshwater ecosystems (Ceola et al., 2013; Fitzhugh & Richter, 2004; Liyanage & Yamada, 2017; Pekel et al., 2016; Poff et al., 1997; Rodell et al., 2018; Sun & Caldwell, 2015). A water-land transition, producing surface water loss and river fragmentation, significantly impacts riverine biodiversity and essential ecosystem services (Botter & Durighetto, 2020; Grill et al., 2019; McDonald, Green, et al., 2011; Pekel et al., 2016). Such degradation of ecosystems and freshwater species has been extensively reported in the CONUS and it is expected to occur in other areas across the globe where the use of land and water is changing and population is growing (Fitzhugh & Richter, 2004). As a result, it is crucial to gain a better understanding of the dynamics of interaction between urbanization and surface water, and in particular how the presence of human settlements influences the progressive loss of surface water resources, to find a balance between urban planning and water management policies that ensure water conservation and ecosystem protection (Hoekstra et al., 2018; McDonald, Douglas, et al., 2011; McGrane, 2016; Paiva et al., 2020; Vörösmarty et al., 2010; Wada et al., 2016).

This study aims at assessing the driving role of urban areas in the spatial distribution of surface water loss across the CONUS. We assumed that irrigation and climatic factors, in particular precipitation change, did not contribute to surface water loss (i.e., water-land transition) that occurred during the period 1984–2018. Indeed, regarding the influence of climate variability on surface water, on average the total annual precipitation and the number of precipitation days have slightly increased in most of the CONUS (Bartels et al., 2018; Easterling et al., 2017; US EPA, 2016), leading to a 0.5% increase of the total surface water area since 1984 (Pekel et al., 2016). Therefore, it is necessary to analyze the influence of urbanization on the spatial distribution of surface water loss, as it is responsible for the emergence of local hotspots that cannot be explained by climate change alone.

To understand the underlying spatial relationship between surface water resources and cities, the extent of built-up areas and the locations of surface water loss were derived from EO data and combined for a spatially explicit modeling analysis. We conducted our analysis under the ideal condition that the spatial interaction between urban areas and surface water resources is solely governed by the geographical distance, disregarding other possible factors of interaction (e.g., roads, piping systems, industrial production, and power generation). We found that at river basin, water resource region, and CONUS levels surface water loss is more frequent close to human settlements and exponentially declines as the distance from urban areas increases. We therefore defined a distance-decay model, described by a truncated exponential probability distribution, that provides a theoretical characterization and a statistically significant modeling of the observed declining trend. Our model demonstrates that urban areas produce an exponentially increasing stress on surface water resources in the proximity of cities. The presence of a steeper distance-decay trend of surface water loss compared to the distance-decay obtained for the overall extent of surface water further confirms that more surface water loss occurred close to urban areas. We also noticed that surface water losses decline faster in river basins with larger urban agglomerations, highlighting that the influence of human settlements increases with the extent of urban clusters.

Distinct patterns in the distance-decay of surface water loss are found across the main Köppen climatic zones (Beck et al., 2018). Localized and concentrated impacts of urban areas on surface water loss are typical of temperate and continental climatic regions, which present larger values of the model's parameters α_b and β_b . Conversely, arid climates are characterized by more distributed impacts, which typically affect larger areas around cities, with smaller α_b and β_b values.

Although the presence of human-managed surface water reservoirs and well fields is not explicitly considered in this analysis, surface water losses associated to such features are implicitly included in our Surface Water Loss map, as specified in the dataset used to derive this map (Pekel et al., 2016). In fact, dams reduce the variability of the downstream river flow (Granzotti et al., 2018), while well fields induce an increase of the groundwater recharge (Xu & Beekman, 2019). Both these effects imply a reduction in surface water extent. To increase the level of detail of the model description and to better understand the role played by dams and groundwater exploitation, further investigations might also inspect the relation between surface water loss and the geographical position of reservoirs and well fields. This additional information may be useful to support the identification of the optimal location of water withdrawals, but a careful assessment will be needed to reach a balance between model complexity and uncertainty.

The probabilistic characterization developed in this work and tested over the CONUS looks promising as it represents a valuable analytical tool that describes the observed spatial distribution of surface water loss locations with

respect to urban areas and provides useful information about the interaction that can potentially be found in other study areas with similar social and climatic conditions. The application of this approach to other regions might reveal the actual capability of our distance-decay model at reproducing the observed spatial interaction between human settlements and surface water depletion, supplying baseline information for the identification of sustainable management practices that guarantee a balance between urban population growth, urban water demand, and water needs for the environment.

Conflict of Interest

Authors Irene Palazzoli and Serena Ceola declare no conflict of interest relevant to this study. Author Alberto Montanari is a member of the editorial board of AGU Advances.

Data Availability Statement

Datasets for this research are available in the corresponding in-text data citation references. Specifically, the Surface Water Transitions layer can be downloaded at <https://global-surface-water.appspot.com/download> and the GHS-BUILT layer at <https://ghsl.jrc.ec.europa.eu/download.php>. The Surface Water Loss and Urbanization maps have been deposited in the Zenodo Digital Repository <http://doi.org/10.5281/zenodo.4472831> (Palazzoli et al., 2021).

References

- Artell, J., Ahtiainen, H., & Pouta, E. (2019). Distance decay and regional statistics in international benefit transfer. *Ecological Economics*, *164*, 106383. <https://doi.org/10.1016/j.ecolecon.2019.106383>
- Averyt, K., Meldrum, J., Caldwell, P., Sun, G., McNulty, S., Huber-Lee, A., & Madden, N. (2013). Sectoral contributions to surface water stress in the coterminous United States. *Environmental Research Letters*, *8*(3), 035046. <https://doi.org/10.1088/1748-9326/8/3/035046>
- Baldocchi, D., Dralle, D., Jiang, C., & Ryu, Y. (2019). How much water is evaporated across California? A multiyear assessment using a biophysical model forced with satellite remote sensing data. *Water Resources Research*, *55*, 2722–2741. <https://doi.org/10.1029/2018WR023884>
- Bartels, R. J., Black, A. W., & Keim, B. D. (2018). Trends in precipitation days in the United States. *International Journal of Climatology*, *40*, 1038–1048. <https://doi.org/10.1002/joc.6254>
- Beck, H. E., Zimmermann, N. E., McVicar, T. R., Vergopolan, N., Berg, A., & Wood, E. F. (2018). Present and future Köppen-Geiger climate classification maps at 1-km resolution. *Scientific Data*, *5*(1). <https://doi.org/10.1038/sdata.2018.214>
- Bigelow, D. P., Plantinga, A. J., Lewis, D. J., & Langpap, C. (2017). How does urbanization affect water withdrawals? Insights from an econometric-based landscape simulation. *Land Economics*, *93*(3), 413–436. <https://doi.org/10.3368/le.93.3.413>
- Boretti, A., & Rosa, L. (2019). Reassessing the projections of the world water development report. *npj Clean Water*, *2*, 15. <https://doi.org/10.1038/s41545-019-0039-9>
- Botter, G., & Durighetto, N. (2020). The stream length duration curve: A tool for characterizing the time variability of the flowing stream length. *Water Resources Research*, *56*, e2020WR027282. <https://doi.org/10.1029/2020WR027282>
- Brown, T. C., Mahat, V., & Ramirez, J. A. (2019). Adaptation to future water shortages in the United States caused by population growth and climate change. *Earth's Future*, *7*, 219–234. <https://doi.org/10.1029/2018EF001091>
- Ceola, S., Hödl, I., Adlboller, M., Singer, G., Bertuzzo, E., Mari, L., et al. (2013). Hydrologic variability affects invertebrate grazing on phototrophic biofilms in stream microcosms. *PLoS One*, *8*(4), e60629. <https://doi.org/10.1371/journal.pone.0060629>
- Ceola, S., Laio, F., & Montanari, A. (2014). Satellite nighttime lights reveal increasing human exposure to floods worldwide. *Geophysical Research Letters*, *41*(20), 7184–7190. <https://doi.org/10.1002/2014gl061859>
- Ceola, S., Laio, F., & Montanari, A. (2019). Global-scale human pressure evolution imprints on sustainability of river systems. *Hydrology and Earth System Sciences*, *23*(9), 3933–3944. <https://doi.org/10.5194/hess-23-3933-2019>
- Chen, Y., & Huang, L. (2018). A scaling approach to evaluating the distance exponent of the urban gravity model. *Chaos, Solitons & Fractals*, *109*, 303–313. <https://doi.org/10.1016/j.chaos.2018.02.037>
- Corbane, C., Pesaresi, M., Kemper, T., Politis, P., Florczyk, A. J., Syrris, V., et al. (2019). Automated global delineation of human settlements from 40 years of Landsat satellite data archives. *Big Earth Data*, *3*, 140–169. <https://doi.org/10.1080/20964471.2019.1625528>
- Daher, B., Lee, S. H., Kaushik, V., Blake, J., Askariyeh, M. H., Shafieezadeh, H., et al. (2019). Towards bridging the water gap in Texas: A water-energy-food nexus approach. *The Science of the Total Environment*, *647*, 449–463. <https://doi.org/10.1016/j.scitotenv.2018.07.398>
- Delpla, I., Jung, A.-V., Baures, E., Clement, M., & Thomas, O. (2009). Impacts of climate change on surface water quality in relation to drinking water production. *Environment International*, *35*(8), 1225–1233. <https://doi.org/10.1016/j.envint.2009.07.001>
- Dieter, C. A., Maupin, M. A., Caldwell, R. R., Harris, M. A., Ivahnenko, T. I., Lovelace, J. K., et al. (2018). Estimated use of water in the United States in 2015: U.S. *Geological Survey Circular*, *1441*, 65. [Supersedes USGS Open-File Report 2017–1131]. <https://doi.org/10.3133/cir1441>
- Duran-Encalada, J. A., Paucar-Caceres, A., Bandala, E. R., & Wright, G. H. (2017). The impact of global climate change on water quantity and quality: A system dynamics approach to the US–Mexican transborder region. *European Journal of Operational Research*, *256*(2), 567–581. <https://doi.org/10.1016/j.ejor.2016.06.016>
- Easterling, D. R., Kunkel, K. E., Arnold, J. R., Knutson, T., LeGrande, A. N., Leung, L. R., et al. (2017). Precipitation change in the United States. In D. J. Wuebbles, D. W. Fahey, K. A. Hibbard, D. J. Dokken, B. C. Stewart, & T. K. Maycock (Eds.), *Climate science special report: Fourth national climate assessment, volume 1* (pp. 207–230). U.S. Global Change Research Program. <https://doi.org/10.7930/J0H993CC>
- Erler, A. R., Frey, S. K., Khader, O., d'Orgeville, M., Park, Y.-J., Hwang, H.-T., et al. (2019). Simulating climate change impacts on surface water resources within a lake-affected region using regional climate projections. *Water Resources Research*, *55*, 130–155. <https://doi.org/10.1029/2018WR024381>

- Fang, Y., Ceola, S., Paik, K., McGrath, G., Rao, P. S. C., Montanari, M., & Jawitz, J. W. (2018). Globally universal fractal pattern of human settlements in river networks. *Earth's Future*, 6, 1134–1145. <https://doi.org/10.1029/2017EF000746>
- Fang, Y., & Jawitz, J. W. (2019). The evolution of human population distance to water in the U.S. from 1790 to 2010. *Nature Communications*, 10, 430. <https://doi.org/10.1038/s41467-019-08366-z>
- Ferguson, I. M., & Maxwell, R. M. (2012). Human impacts on terrestrial hydrology: Climate change versus pumping and irrigation. *Environmental Research Letters*, 7, 044022. <https://doi.org/10.1088/1748-9326/7/4/044022>
- Figueiredo, O., Guimarães, P., & Woodward, D. (2015). Industry localization, distance decay, and knowledge spillovers: Following the patent paper trail. *Journal of Urban Economics*, 89, 21–31. <https://doi.org/10.1016/j.jue.2015.06.003>
- Fitzhugh, T. W., & Richter, B. D. (2004). Quenching urban thirst: Growing cities and their impacts on freshwater ecosystems. *BioScience*, 54(8), 741. [https://doi.org/10.1641/0006-3568\(2004\)054\[0741:qutgca\]2.0.co;2](https://doi.org/10.1641/0006-3568(2004)054[0741:qutgca]2.0.co;2)
- Flörke, M., Schneider, C., & McDonald, R. I. (2018). Water competition between cities and agriculture driven by climate change and urban growth. *Nature Sustainability*, 1, 51–58. <https://doi.org/10.1038/s41893-017-0006-8>
- Fotheringham, A. S. (1981). Spatial structure and distance-decay parameters. *Annals of the Association of American Geographers*, 71(3), 425–436. <https://doi.org/10.1111/j.1467-8306.1981.tb01367.x>
- Goldmann, K., Schröter, K., Pena, R., Schöning, I., Schrupf, M., Buscot, F., et al. (2016). Divergent habitat filtering of root and soil fungal communities in temperate beech forests. *Scientific Reports*, 6, 31439. <https://doi.org/10.1038/srep31439>
- Granzotti, R. V., Miranda, L. E., Agostinho, A. A., & Gomes, L. C. (2018). Downstream impacts of dams: Shifts in benthic invertivorous fish assemblages. *Aquatic Sciences*, 80, 28. <https://doi.org/10.1007/s00027-018-0579-y>
- Grill, G., Lehner, B., Thieme, M., Geenen, B., Tickner, D., Antonelli, F., et al. (2019). Mapping the world's free-flowing rivers. *Nature*, 569, 215–221. <https://doi.org/10.1038/s41586-019-1111-9>
- Haddeland, I., Skaugen, T., & Lettenmaier, D. P. (2006). Anthropogenic impacts on continental surface water fluxes. *Geophysical Research Letters*, 33, L08406. <https://doi.org/10.1029/2006GL026047>
- Halás, M., Klapka, P., & Kládivo, P. (2014). Distance-decay functions for daily travel-to-work flows. *Journal of Transport Geography*, 35, 107–119. <https://doi.org/10.1016/j.jtrangeo.2014.02.001>
- Hoekstra, A. Y., Buurman, J., & van Ginkel, K. C. H. (2018). Urban water security: A review. *Environmental Research Letters*, 13(5), 053002. <https://doi.org/10.1088/1748-9326/aaba52>
- Huang, C., Chen, Y., Zhang, S., & Wu, J. (2018). Detecting, extracting, and monitoring surface water from space using optical sensors: A review. *Reviews of Geophysics*, 56(2), 333–360. <https://doi.org/10.1029/2018RG000598>
- Jenkins, W. A., Murray, B. C., Kramer, R. A., & Faulkner, S. P. (2010). Valuing ecosystem services from wetlands restoration in the Mississippi Alluvial Valley. *Ecological Economics*, 69(5), 1051–1061. <https://doi.org/10.1016/j.ecolecon.2009.11.022>
- Khatri, N., & Tyagi, S. (2015). Influences of natural and anthropogenic factors on surface and groundwater quality in rural and urban areas. *Frontiers in Life Science*, 8(1), 23–39. <https://doi.org/10.1080/21553769.2014.933716>
- Li, B., Gao, S., Liang, Y., Kang, Y., Prestby, T., Gao, Y., & Xiao, R. (2020). Estimation of regional economic development indicator from transportation network analytics. *Scientific Reports*, 10, 2647. <https://doi.org/10.1038/s41598-020-59505-2>
- Li, C., Sun, G., Caldwell, P. V., Cohen, E., Fang, Y., Zhang, Y., et al. (2020). Impacts of urbanization on watershed water balances across the conterminous United States. *Water Resources Research*, 56, e2019WR026574. <https://doi.org/10.1029/2019WR026574>
- Liu, X., Yang, K., Bennet, M. M., Lu, X., Guo, Z., & Li, M. (2021). Changes to anthropogenic pressures on reach-scale rivers in South and Southeast Asia from 1990 to 2014. *Environmental Research Letters*, 16(1), 014025. <https://doi.org/10.1088/1748-9326/abc77>
- Liu, X., Huang, Y., Xu, X., Li, X., Li, X., Ciais, P., et al. (2020). High-spatiotemporal-resolution mapping of global urban change from 1985 to 2015. *Nature Sustainability*, 3, 564–570. <https://doi.org/10.1038/s41893-020-0521-x>
- Liyanaage, C. P., & Yamada, K. (2017). Impact of population growth on the water quality of natural water bodies. *Sustainability*, 9, 1405. <https://doi.org/10.3390/su9081405>
- Lyons, W. B. (2014). Water and urbanization. *Environmental Research Letters*, 9, 111002. <https://doi.org/10.1088/1748-9326/9/11/11002>
- Marconcini, M., Metz-Marconcini, A., Üreyen, S., Palacios-Lopez, D., Hanke, W., Bachofer, F., et al. (2020). Outlining where humans live, the world settlement footprint 2015. *Scientific Data*, 7, 242. <https://doi.org/10.1038/s41597-020-00580-5>
- Mård, J., Di Baldassarre, G., & Mazzoleni, M. (2018). Nighttime light data reveal how flood protection shapes human proximity to rivers. *Science Advances*, 4, 5779–5801. <https://doi.org/10.1126/sciadv.aar5779>
- Martínez, L. M., & Viegas, J. M. (2013). A new approach to modelling distance-decay functions for accessibility assessment in transport studies. *Journal of Transport Geography*, 26, 87–96. <https://doi.org/10.1016/j.jtrangeo.2012.08.018>
- McDonald, R. I., Douglas, I., Revenga, C., Hale, R., Grimm, N., Grönwall, J., & Fekete, B. (2011). Global urban growth and the geography of water availability, quality, and delivery. *Ambio*, 40, 437–446. <https://doi.org/10.1007/s13280-011-0152-6>
- McDonald, R. I., Green, P., Balk, D., Fekete, B. M., Revenga, C., Todd, M., & Montgomery, M. (2011). Urban growth, climate change, and freshwater availability. *Proceedings of the National Academy of Sciences*, 108(15), 6312–6317. <https://doi.org/10.1073/pnas.1011615108>
- McDonald, R. I., Weber, K., Padowski, J., Flörke, M., Schneider, C., Green, P. A., et al. (2014). Water on an urban planet: Urbanization and the reach of urban water infrastructure. *Global Environmental Change*, 27, 96–105. <https://doi.org/10.1016/j.gloenvcha.2014.04.022>
- McGrane, S. J. (2016). Impacts of urbanisation on hydrological and water quality dynamics, and urban water management: A review. *Hydrological Sciences Journal*, 61, 2295–2311. <https://doi.org/10.1080/02626667.2015.1128084>
- Okello, C., Tomasello, B., Greggio, N., Wambiji, N., & Antonellini, M. (2015). Impact of population growth and climate change on the freshwater resources of lamu island, Kenya. *Water*, 7, 1264–1290. <https://doi.org/10.3390/w7031264>
- Padowski, J. C., & Gorelick, S. M. (2014). Global analysis of urban surface water supply vulnerability. *Environmental Research Letters*, 9, 104004. <https://doi.org/10.1088/1748-9326/9/11/119501>
- Padowski, J. C., & Jawitz, J. W. (2012). Water availability and vulnerability of 225 large cities in the United States. *Water Resources Research*, 48, W12529. <https://doi.org/10.1029/2012WR012335>
- Paiva, A. C. D. E., Nascimento, N., Rodriguez, D. A., Tomasella, J., Carriello, F., & Rezende, F. S. (2020). Urban expansion and its impact on water security: The case of the Paraíba do Sul River Basin, São Paulo, Brazil. *The Science of the Total Environment*, 720, 137509. <https://doi.org/10.1016/j.scitotenv.2020.137509>
- Palazzoli, I., Montanari, A., & Ceola, S. (2021). Surface water loss map and urbanization map. *Zenodo*. <https://doi.org/10.5281/zenodo.4472831>
- Pekel, J. F., Cottam, A., Gorelick, N., & Belward, A. S. (2016). High-resolution mapping of global surface water and its long-term changes. *Nature*, 540, 418–422. <https://doi.org/10.1038/nature20584>
- Poff, N. L., Allan, J. D., Bain, M. B., Karr, J. R., Prestegard, K. L., Richter, B. D., et al. (1997). The natural flow regime. *BioScience*, 47(11), 769–784. <https://doi.org/10.2307/1313099>

- Richter, B. D., Abell, D., Bacha, E., Brauman, K., Calos, S., Cohn, A., et al. (2013). Tapped out: How can cities secure their water future? *Water Policy*, 15(3), 335–363. <https://doi.org/10.2166/wp.2013.105>
- Rodell, M., Famiglietti, J. S., Wiese, D. N., Reager, J. T., Beaudoing, H. K., Landerer, F. W., & Lo, M.-H. (2018). Emerging trends in global freshwater availability. *Nature*, 557, 651–659. <https://doi.org/10.1038/s41586-018-0123-1>
- Seaber, P. R., Kapinos, F. P., & Knapp, G. L. (1987). Hydrologic unit maps. In *U.S. Geological survey water supply paper 2294*. <https://doi.org/10.3133/wsp2294>
- Smedema, L. K., Abdel-Dayem, S., & Ochs, W. J. (2000). Drainage and agricultural development. *Irrigation and Drainage Systems*, 14, 223–235. <https://doi.org/10.1023/A:1026570823692>
- Sun, G., & Caldwell, P. (2015). Impacts of urbanization on stream water quantity and quality in the United States. *Water Resources IMPACT*, 17(1), 17–20. Retrieved from <https://www.jstor.org/stable/wateresoimpa.17.1.0017>
- Taylor, P. J. (1971). Distance transformation and distance-decay function. *Geographical Analysis*, 3(3), 221–238. <https://doi.org/10.1111/j.1538-4632.1971.tb00364.x>
- United Nations, Department of Economic and Social Affairs, Population Division. (2019). *World urbanization prospects: The 2018 revision (ST/ESA/SER.A/420)*. United Nations.
- US Census. (2021). *Urbanized areas and urban clusters: 2010*. Retrieved from https://www.census.gov/library/visualizations/2010/geo/ua2010_uas_and_ucs_map.html
- US EPA. (2016). *Climate change indicators in the United States: U.S. and global precipitation* (4th ed.). U.S. Environmental Protection Agency. Retrieved from <https://www.epa.gov/climate-indicators>
- Vörösmarty, C., McIntyre, P. B., Gessner, M. O., Dudgeon, D., Prusevich, A., Green, P., et al. (2010). Global threats to human water security and river biodiversity. *Nature*, 467, 555–561. <https://doi.org/10.1038/nature09440>
- Wada, Y., Flörke, M., Hanasaki, N., Eisner, S., Fischer, G., Tramberend, S., et al. (2016). Modeling global water use for the 21st century: The water futures and solutions (WFaS) initiative and its approaches. *Geoscientific Model Development*, 9, 175–222. <https://doi.org/10.5194/gmd-9-175-2016>
- Wada, Y., van Beek, L. P. H., & Bierkens, M. F. P. (2012). Nonsustainable groundwater sustaining irrigation: A global assessment. *Water Resources Research*, 48(6). <https://doi.org/10.1029/2011wr010562>
- Wada, Y., van Beek, L. P. H., Wanders, N., & Bierkens, M. F. P. (2013). Human water consumption intensifies hydrological drought worldwide. *Environmental Research Letters*, 8(3), 034036. <https://doi.org/10.1088/1748-9326/8/3/034036>
- Xiong, L., Deng, R., Li, J., Liu, X., Qin, Y., Liang, Y., & Liu, Y. (2018). Subpixel surface water extraction (SSWE) using Landsat 8 OLI data. *Water*, 10(5), 653. <https://doi.org/10.3390/w10050653>
- Xu, Y., & Beekman, H. E. (2019). Review: Groundwater recharge estimation in arid and semi-arid southern Africa. *Hydrogeology Journal*, 27, 929–943. <https://doi.org/10.1007/s10040-018-1898-8>
- Yamazaki, D., & Trigg, M. A. (2016). Hydrology: The dynamics of Earth's surface water. *Nature*, 540, 348–349. <https://doi.org/10.1038/nature21100>
- Yizaw, W., & Hossain, F. (2016). Water sustainability of large cities in the United States from the perspectives of population increase, anthropogenic activities, and climate change. *Earth's Future*, 4, 603–617. <https://doi.org/10.1002/2016EF000393>
- Yin, Z.-C., Jin, Z.-H.-N., Ying, S., Liu, H., Li, S.-J., & Xiao, J.-Q. (2019). Distance-decay effect in probabilistic time geography for random encounter. *ISPRS International Journal of Geo-Information*, 8(4), 177. <https://doi.org/10.3390/ijgi8040177>
- Zhang, T. (2011). Distance-decay patterns of nutrient loading at watershed scale: Regression modeling with a special spatial aggregation strategy. *Journal of Hydrology*, 402(3–4), 239–249. <https://doi.org/10.1016/j.jhydrol.2011.03.017>
- Zhou, D., Zhao, S., Zhang, L., Sun, G., & Liu, Y. (2015). The footprint of urban heat island effect in China. *Scientific Reports*, 5(1), 1–11. <https://doi.org/10.1038/srep11160>